

VIBRATION REDUCTION IN HINGELESS ROTORS USING AN
ACTIVELY CONTROLLED FLAP AND ITS IMPLEMENTATION USING
MAGNETOSTRICTIVE ACTUATION

by

T.A. Milllott and P.P. Friedmann

MECHANICAL, AEROSPACE AND NUCLEAR ENGINEERING
DEPARTMENT, UNIVERSITY OF CALIFORNIA
LOS ANGELES, CALIFORNIA, USA

TWENTIETH EUROPEAN ROTORCRAFT FORUM
OCTOBER 4 - 7, 1994 AMSTERDAM

VIBRATION REDUCTION IN HINGELESS ROTORS USING AN ACTIVELY CONTROLLED FLAP AND ITS IMPLEMENTATION USING MAGNETOSTRICTIVE ACTUATION

Thomas A. Millott and Peretz P. Friedmann
Mechanical, Aerospace and Nuclear Engineering Department
University of California, Los Angeles, CA 90024

Abstract

This paper describes a comprehensive study of vibration reduction in a four-bladed helicopter rotor using an actively controlled flap (ACF) located on the blade. This sequel to an earlier feasibility study utilizes a flexible blade model to examine the practical implementation of the ACF. A deterministic feedback controller is implemented to reduce the 4/rev hub loads. Comparisons with individual blade control (IBC), in which the entire blade is oscillated in pitch, show that the ACF is comparable to IBC in its vibration reduction effectiveness, but requires substantially less power for its implementation. A comprehensive set of trend studies are conducted and it is found that the torsional stiffness of the blade, the ACF spanwise location, and the chordwise offset of the ACF center of gravity from the hinge axis are important parameters. Time domain simulations of the helicopter response to control are carried out to investigate the validity of the quasistatic assumption frequently used in vibration reduction studies. Finally, implementation of the ACF using magnetostrictive actuation technology is considered and found to be a viable approach.

Nomenclature

a	Compressible lift curve slope
a_o	Incompressible lift curve slope
c_b	Blade chord
C_f	Hinge moment correction factor
C_{do}	Blade drag coefficient
C_{mo}	Blade moment coefficient
C_w	Weight coefficient = $\text{Weight}/\pi R^2 \rho_A R^2 \Omega^2$
D	Control matrix
e	Blade root offset
ERR	Error control parameter
f_b	Vector of blade equations
f_t	Vector of trim equations
fC_{df}	Fuselage flat plate drag area
g_b	$= f_b - M \ddot{q}_b$
I_{MB2}, I_{MB3}	Principal mass moments of inertia
J	Quadratic cost functional
L_b	Blade length
M_b	Total mass of one blade
M_H	Control surface hinge moment
M_{tip}	Blade tip Mach number in hover
M_x	Blade root feathering moment
$M_{x,\psi}$	Mach number on blade at x, ψ
N_b	Number of blades in the rotor
P_{cs}	ACF power

P_{IBC}	IBC power
\mathbf{q}_b	Vector of blade dofs
\mathbf{q}_t	Vector of trim parameters
R	Rotor radius
t	Time
t_s	Update period of closed-loop controller
T	Rotor period, = $\Omega/2\pi$
\mathbf{T}	Transfer matrix relating vibratory response to control
\mathbf{u}_i	Vector of control input harmonics
$\mathbf{W}_z, \mathbf{W}_u, \mathbf{W}_\Delta$	Weighting matrices in quadratic cost functional
x_c	Spanwise location of ACF centroid
\mathbf{y}	State vector, = $\{\mathbf{q}_b^T \dot{\mathbf{q}}_b^T\}^T$
\mathbf{z}_i	N_b /rev vibration harmonics
\mathbf{z}_0	Baseline value of \mathbf{z}_i

Greek Symbols

β	Prandtl-Glauert compressibility correction factor
δ	Control flap deflection angle
γ	Lock number
θ_{IBC}	IBC pitch input
μ	Advance ratio
ρ_A	Air density
ψ	Blade azimuth angle
Ω	Rotor angular velocity
ω_{F1}, ω_{L1}	First rotating flap, lead-lag and torsional frequencies, respectively
ω_{T1}	
ω_{F2}, ω_{L2}	Second rotating flap and lead-lag frequencies, respectively
σ	Blade solidity ratio

Special Symbols

$(\cdot)_{,x}$	Derivative w.r.t. spanwise coordinate x
$(\dot{\cdot})$	Derivative w.r.t. time

1. Introduction and Problem Statement

The desire to reduce vibrations to levels below those attainable by passive means[1,2] has motivated the use of active controls for vibration reduction. One such approach, commonly denoted as higher harmonic control[3] (HHC), has emerged as a potential candidate for implementation in production helicopters. In this approach, additional collective and cyclic pitch inputs at frequencies greater than 1/rev (used for flight control) are introduced in the fixed system through an actively controlled conventional swashplate. This approach attempts to reduce vibrations in the fuselage, or at the hub, by tailoring the vibratory aerodynamic loads on the blades; thus modifying them at their source, before they propagate to the airframe. The validity of this approach for producing substantial vibration reduction has been demonstrated by analytical simulations[5-10], wind tunnel tests[11-13] and flight tests[14-16].

The alternative approach denoted individual blade control[17] (IBC) yields an improvement in vibration reduction compared to HHC by controlling the pitch angle of each blade independently in the rotating frame. This approach removes some of the limitations which exist in active control through a conventional swashplate, but a

more complex control system is required, including the possibility of replacing the conventional swashplate by an "electronic swashplate"[18,19].

It is noteworthy that both HHC and IBC introduce the pitch control for vibration reduction through the primary flight control system of the helicopter, and therefore the presence of such an active vibration control device introduces some constraints on the system, from an airworthiness point of view. Furthermore, comparison studies[8,9] of HHC carried out for equivalent articulated and hingeless rotors have indicated the existence of significant power penalty associated with the need to drive harmonically the coupled structural dynamic system represented by the hingeless blade. Similar restrictions may be valid for the case of IBC, which also involves oscillating the entire blade.

Inspired by the successful experience at Kaman with mechanically controlled flaps mounted on blades[20], the feasibility of using an actively controlled partial span flap, shown in Fig. 1(a), for vibration reduction was explored in Ref. 21. This feasibility study, based on a simple offset-hinged spring restrained blade model with coupled flap-lag-torsional dynamics, demonstrated the capability of the ACF for producing roughly the same degree of vibration reduction as IBC (in which the entire blade is oscillated), while consuming only 12-20% of the power required by IBC.

Encouraged by these results a second stage of this study was undertaken, emphasizing the practical aspects of the implementing the ACF on a hingeless rotor. This paper, which describes the results obtained in the second stage, has a number of specific objectives, described below.

(1) Implement the actively controlled partial span flap with a fully elastic, geometrically nonlinear, blade model in which the dynamics of the blade are represented by two torsional, two chordwise bending and three flapwise bending modes.

(2) Study the sensitivity of the vibration reduction effectiveness of the ACF to the following: (a) spanwise location of the control flap; (b) the torsional stiffness of the blade; (c) the chordwise offset of the control flap c.g. from the hinge axis; (d) the aerodynamic hinge moment correction factor; and (e) compressibility effects.

(3) Examine time domain simulations of the helicopter response to control to determine the validity of the quasistatic assumption commonly made in helicopter vibration reduction studies.

(4) Study the feasibility of implementing this highly effective blade control concept using magnetostrictive type actuation.

2. Mathematical Model

A fully elastic blade model, shown in Fig. 1(b), with fully coupled flap, lead-lag and torsional dynamics is selected to represent the hingeless blade. The structural part of the flexible blade model is taken from Ref. 23, which presents a set of nonlinear partial differential equations of motion for a flexible blade undergoing fully coupled flap-lag-torsional dynamics with moderate deflections. A complete and detailed description of the derivation of the equations of motion can be found in Ref. 24.

The inertial loads are determined using D'Alembert's principle. An appropriately modified version of Greenberg's quasisteady aerodynamic theory[25] incorporating the effects of an aerodynamic control surface is used to obtain the aerodynamic loads on the blade. A detailed description of this modification is beyond the scope of this paper, and the final expressions have already been presented in Ref. 21. Reverse flow is included but dynamic stall effects are neglected. Compressibility effects are either neglected, or accounted for using the Prandtl-Glauert correction factor

$\beta = \sqrt{1 - M_{x,\psi}^2}$ to obtain the compressible lift curve slope $a = a_0/\beta$, where $M_{x,\psi}$ is the local Mach number at x, ψ .

The structural, inertial and aerodynamic loads are developed explicitly using the symbolic manipulation program MACSYMA[24,26]. A description of the use of MACSYMA to formulate the blade loads, and a list of the resulting explicit expressions, can be found in Ref. 24. Moderate deflections are assumed in the formulation; thus the equations of motion of the blade contain geometrically nonlinear terms in the structural, inertial and aerodynamic operators associated with this aeroelastic problem. An ordering scheme is employed to keep the size of the explicit expressions to a manageable size[27]. The ordering scheme is based on the assumption that

$$1 + O(\varepsilon^2) \approx 1 \quad (1)$$

where ε is a small dimensionless parameter on the order of typical blade bending slopes ($0.1 \leq \varepsilon \leq 0.2$). Such an ordering scheme is particularly convenient when combined with a symbolic manipulator such as MACSYMA[24].

The aerodynamic lift and moment associated with the presence of a trailing edge flap are modified by an empirical hinge moment correction factor C_f , where $0.0 < C_f < 1.0$, that accounts for the presence of a gap between the trailing edge of the blade and the leading edge of the flap, which is not modeled in this study. Experimental data[28,29] indicate that flap effectiveness can vary by as much as 50% due to the presence of such a gap.

The spatial dependence in the equations of motion is removed using Galerkin's method of weighted residuals based on two torsion, two lead-lag, and three flap free vibration modes of a rotating, uniform, cantilevered blade. The rotating modes are obtained from the exact nonrotating mode shapes of a uniform cantilevered beam. The resulting coupled ordinary nonlinear differential equations of motion can be conveniently written in vector form

$$\mathbf{f}_b(\mathbf{q}_b, \dot{\mathbf{q}}_b, \ddot{\mathbf{q}}_b, \mathbf{q}_t, \delta; \psi) = \mathbf{0} \quad (2)$$

The vector \mathbf{q}_t contains the quantities governing the trim state of the helicopter, for propulsive trim, which are obtained from the solution of

$$\mathbf{f}_t(\mathbf{q}_b, \dot{\mathbf{q}}_b, \ddot{\mathbf{q}}_b, \mathbf{q}_t, \delta; \psi) = \mathbf{0} \quad (3)$$

which represents the requirement for longitudinal and vertical force equilibrium as well as pitch and roll equilibrium of the helicopter in steady, level flight. In Eqs. (3) the uniform inflow is calculated from[33]

$$\lambda - \mu \tan(\alpha_R) - \frac{C_T}{2\sqrt{\lambda^2 + \mu^2}} = 0 \quad (4)$$

Note that in these and the following equations bold type indicates vector or matrix quantities.

3. Method of Solution

3.1 Frequency Domain Approach

The harmonic balance technique (HBT) is used to calculate the trim state and equilibrium solution of the blade in a coupled manner; this approach is usually denoted coupled trim/aeroelastic analysis. The blade response in steady forward flight is periodic with a fundamental frequency equal to the rotor speed Ω , and thus it can be approximated by a truncated Fourier expansion containing N_H harmonics

$$\mathbf{q}_b = \mathbf{q}_{b0} + \sum_{n=1}^{N_H} [\mathbf{q}_{bnc} \cos(n\psi_k) + \mathbf{q}_{bns} \sin(n\psi_k)] \quad (5)$$

where the number of harmonics N_H retained determines the quality of this approximate solution.

The blade equations of motion, Eqs. (2), represent a periodic system and thus can also be approximated by a truncated Fourier series expansion

$$\mathbf{f}_b = \mathbf{f}_{b0} + \sum_{n=1}^{N_H} [\mathbf{f}_{bnc} \cos(n\psi_k) + \mathbf{f}_{bns} \sin(n\psi_k)] \quad (6)$$

An approximate solution to the blade equations can be obtained from the requirement that the constant part as well as the first N_H harmonics in Eq. (6) be zero:

$$\mathbf{f}_{b0} = \frac{1}{2\pi} \int_0^{2\pi} \mathbf{f}_b(\mathbf{q}_b, \dot{\mathbf{q}}_b, \ddot{\mathbf{q}}_b, \mathbf{q}_t, \delta; \psi) d\psi = 0 \quad (7)$$

and for $1 \leq n \leq N_H$

$$\mathbf{f}_{bnc} = \frac{1}{\pi} \int_0^{2\pi} \mathbf{f}_b(\mathbf{q}_b, \mathbf{q}_t, \delta; \psi) \cos(n\psi) d\psi = 0 \quad (8)$$

$$\mathbf{f}_{bns} = \frac{1}{\pi} \int_0^{2\pi} \mathbf{f}_b(\mathbf{q}_b, \mathbf{q}_t, \delta; \psi) \sin(n\psi) d\psi = 0 \quad (9)$$

Similarly, the trim equations, Eqs. (3), can also be approximated by the truncated Fourier series expansion

$$\mathbf{f}_t = \mathbf{f}_{t0} + \sum_{n=1}^{N_H} [\mathbf{f}_{tnc} \cos(n\psi) + \mathbf{f}_{tns} \sin(n\psi)] \quad (10)$$

Enforcing the trim condition for straight and level flight at fixed advance ratio implies that only the constant part of the forces and moments acting on the vehicle have to satisfy the equilibrium condition. Therefore only the constant part of Eq. (3) needs to be satisfied

$$\mathbf{f}_{t0} = \frac{1}{2\pi} \int_0^{2\pi} \mathbf{f}_t(\mathbf{q}_b, \dot{\mathbf{q}}_b, \ddot{\mathbf{q}}_b, \mathbf{q}_t, \delta; \psi) d\psi = 0 \quad (11)$$

Using the HBT to solve the coupled trim aeroelastic response problem requires the iterative solution of the nonlinear algebraic system represented by Eqs. (7) – (9) and (11) for the vector of trim variables \mathbf{q}_t and the $(1 + 2N_H)$ Fourier coefficient vectors represented by \mathbf{q}_{b0} , \mathbf{q}_{bnc} , and \mathbf{q}_{bns} ($1 \leq n \leq N_H$). The same number of harmonics is retained in both Eqs. (5) and (6) so that the system contains the same number of equations as unknowns. Since the ultimate goal is to determine the 4/rev vibratory hub loads, at least four harmonics should be retained in the expansion. Also, to properly capture the effects of the various N/rev harmonic inputs, N_H should be at least one greater than the highest harmonic used in the control input.

Gaussian quadrature is used to perform the integrations in Eqs. (7) – (9) and (11). Equation (5) is not substituted directly into Eqs. (7) – (9) and (11), but is instead evaluated numerically at each ψ required by the numerical integration scheme. The IMSL subroutine DNEQNF[30], which solves systems of non-linear algebraic equations, is used to obtain the coupled trim and response solution.

3.2 Time Domain Solution

The HBT is convenient for simultaneously extracting the trim and aeroelastic response solution. However, only the steady state solution is generated, and thus one can only simulate the implementation of discrete time controllers. This precludes application of many modern control approaches which have been developed for continuous time systems. Furthermore, since the HBT provides only the steady state response, the problem of transient system dynamics and its control cannot be addressed.

Therefore, in this section direct solution of the nonlinear ordinary differential equations of motion of the blade in the time domain is examined using a general purpose ordinary differential equation (ODE) solver DE/STEP[31]. In this approach the entire time history of the system response is available for control applications. The algorithm implemented in DE/STEP is a variant of the Adams-Bashforth method, in which the integration step size is selected such that each component of the local error vector \mathbf{e}_{local} satisfies

$$|\mathbf{e}_{local}(i)| \leq \text{RELERR} \times |\mathbf{y}(i)| + \text{ABSERR}$$

where RELERR and ABSERR are the relative and absolute error bounds, respectively, specified by the user. A combined error criterion is usually best[31], so in this study $\text{ERR} = \text{RELERR} = \text{ABSERR}$.

To use the ODE solver the equations of motion must be expressed in first order form $\dot{\mathbf{y}} = \mathbf{F}(\mathbf{y}, t)$. The second order differential equations of motion of the blade, represented by Eq. (2), can be converted to first order form by decomposing the blade equations as indicated below

$$\mathbf{f}_b = \mathbf{g}_b(\mathbf{q}_b, \dot{\mathbf{q}}_b, \mathbf{q}_t; t) + \mathbf{M} \ddot{\mathbf{q}}_b = \mathbf{0} \quad (12)$$

The matrix \mathbf{M} is identical to the mass matrix obtained from a linearization of the equations about the response. The vector \mathbf{g}_b is the component of the blade equations which is independent of the acceleration vector $\ddot{\mathbf{q}}_b$. The decomposition of the blade equations \mathbf{f}_b represented by Eq. (12) is performed explicitly using the symbolic manipulation software MACSYMA[24].

Solving Eq. (12) for $\ddot{\mathbf{q}}_b$, the first order, state variable form of the equations can be expressed as:

$$\dot{\mathbf{y}} = \begin{Bmatrix} \dot{\mathbf{q}}_b \\ \ddot{\mathbf{q}}_b \end{Bmatrix} = \begin{bmatrix} \mathbf{0} & \mathbf{I} \\ \mathbf{0} & \mathbf{0} \end{bmatrix} \begin{Bmatrix} \mathbf{q}_b \\ \dot{\mathbf{q}}_b \end{Bmatrix} + \begin{Bmatrix} \mathbf{0} \\ -\mathbf{M}^{-1}\mathbf{g}_b \end{Bmatrix} \quad (13)$$

which is in the appropriate form $\dot{\mathbf{y}} = \mathbf{F}(\mathbf{y}, t)$. The matrix inversion \mathbf{M}^{-1} required to generate Eq. (13) is performed numerically in the FORTRAN code.

When solving the response problem directly in the time domain the order of the system is doubled; however, comparing this to the HBT leads one to conclude that this approach requires much less memory storage and bookkeeping than the HBT. Furthermore, availability of the time domain response facilitates the application of modern control techniques.

3.3 Simplified Trim Procedure

A possible deficiency of the time domain solution approach may be associated with the need to solve the trim and response problems separately. One approach to solving these two problems simultaneously, in the time domain, is commonly denoted the "auto-pilot" method[32]. In this approach a fictitious feedback system (i.e., a numerical controller) is used to trim the helicopter automatically as the equations are integrated in time. Procedures[32] developed thus far, however, demonstrate acceptable convergence characteristics only for torsionally stiff blades.

Instead of using the "auto-pilot" approach, a simplified version of the aeroelastic analysis developed in this study is used to calculate, with sufficient accuracy, the steady state trim settings of the rotor needed as input to the time domain solution procedure. The simplified analysis employs only the fundamental flap, lead-lag and torsional rotating modes for modeling the blade dynamics. Furthermore, only two harmonics are retained in the expansion of the blade degrees of freedom. Comparisons with HBT results, presented later in this study, demonstrate that this simplified aeroelastic analysis yields accurate trim solutions, at a fraction of the computer time needed for implementation with the complete model.

3.4 Vibratory Hub Loads Calculation

Once the trim and aeroelastic response have been obtained, the force and moment at the hub due to the individual blade can be determined by integrating the distributed forces and moments along the span of the blade in the rotating frame, and transforming them to the nonrotating, hub-fixed system. The total hub loads are then calculated by summing the contribution from each blade in the rotor, using a time delay of $2\pi(k-1)/N_b$ to obtain the contribution from the k^{th} blade. A harmonic analysis is then performed; for a four-bladed rotor the principal contribution to the vibratory hub loads is the 4/rev vibratory component.

4. Vibration Reduction Using Active Control

The majority of vibration reduction investigations[5-19] to date have used a frequency domain control approach based on the minimization of a quadratic performance index J given by

$$J = \mathbf{z}_i^T \mathbf{W}_z \mathbf{z}_i + \mathbf{u}_i^T \mathbf{W}_u \mathbf{u}_i + \Delta \mathbf{u}_i^T \mathbf{W}_\Delta \Delta \mathbf{u}_i \quad (14)$$

where $\Delta \mathbf{u}_i = \mathbf{u}_i - \mathbf{u}_{i-1}$. The index i is used here to indicate the discrete time nature of control solutions based on frequency domain formulations. Typically, the vectors \mathbf{z}_i and \mathbf{u}_i contain the harmonics of the vibrations and control input, respectively, dur-

ing the i^{th} time step of the discrete time controller. The time t_s between control updates must be sufficient to allow the system to return to a steady state condition, which may require one or more rotor revolutions. The matrices \mathbf{W}_z , \mathbf{W}_u and \mathbf{W}_Δ represent weighting matrices on the vibrations, control amplitudes, and rate of change of the control, respectively.

A deterministic optimal control law is obtained by taking the partial derivative of J given by Eq. (14) with respect to \mathbf{u}_i and setting this equal to zero

$$\frac{\partial J}{\partial \mathbf{u}_i} = \mathbf{0} \quad (15)$$

and then solving for the optimal control \mathbf{u}_i^* .

In this study a linear, quasistatic, frequency domain representation of the helicopter response to control is used. This type of representation has been used in many previous studies[5-19]. Though in general the response of the helicopter to control is nonlinear, a linear approximation can be obtained by linearizing the system about the current control

$$\mathbf{z}_i = \mathbf{z}_{i-1} + \mathbf{T}\Delta\mathbf{u}_i \quad (16)$$

Substituting Eq. (16) into Eq. (14) and minimizing with respect to the control yields

$$\mathbf{u}_{i+1}^* = \mathbf{u}_i^* + \mathbf{D}^{-1}(-\mathbf{T}^T\mathbf{W}_z\mathbf{z}_i - \mathbf{W}_u\mathbf{u}_i^*) \quad (17)$$

where

$$\mathbf{D} = \mathbf{T}^T\mathbf{W}_z\mathbf{T} + \mathbf{W}_u + \mathbf{W}_\Delta \quad (18)$$

Equation (17) is in the form of a closed-loop controller[4] where the control input during each time step is determined by feedback of the vibration levels.

5. Control Power Requirements

The instantaneous power required to drive the control flap, averaged over one rotor revolution, and multiplied by the number of blades

$$P_{cs} = \sum_{k=1}^{N_b} \frac{1}{2\pi} \int_0^{2\pi} M_H(\psi_k) \dot{\delta}(\psi_k) d\psi_k \quad (19)$$

is used as a measure of the power required to implement the ACF.

The power required to implement IBC is defined as the average power needed to drive the blade root pitch actuators during each revolution

$$P_{IBC} = \sum_{k=1}^{N_b=4} \frac{1}{2\pi} \int_0^{2\pi} M_x(\psi_k) \dot{\theta}_{IBC}(\psi_k) d\psi_k \quad (20)$$

6. Results and Discussion

6.1. Model Verification

Before conducting the active control studies, the flexible blade model (without the control flap) and the solution procedure used in this study were carefully validated by comparing results with Refs. 8 and 34, which employed flexible blade models similar to the one used in this study. Comparisons of trim and response results with Ref. 34, and blade stability and 4/rev hub loads with Ref. 8, are presented in detail in Ref. 24.

6.2. Active Control Studies

The feedback control law given by Eq. (17) was employed to produce simultaneous reduction in the vibratory hub shears and moments using the ACF. Conventional IBC was also implemented for comparison. The input signal consists of 2, 3, 4, and 5/rev harmonic components in the rotating reference frame. This combination of frequencies was found[24] to produce the greatest degree of reduction in the 4/rev hub loads without producing significant increases in the 8/rev hub loads, the next largest component of the vibratory loads in a four-bladed rotor.

In the vibration reduction studies presented in this paper, only the vibration levels were penalized in the quadratic cost functional J (i.e. $\mathbf{W}_u = \mathbf{W}_\Delta = \mathbf{0}$). In this case, J consists of the weighted sum of the squares of the amplitudes of the hub shears and hub moments, and thus represents a measure of the vibration levels experienced during the i^{th} control step. The weightings on the squares of the hub moment amplitudes were scaled by a factor of ten relative to the weightings on the squares of the hub shear amplitudes. This was found to be necessary to produce roughly the same level of reduction in the hub shear and moment components.

The nominal data for the flexible blade configuration employed in this study is presented in Table 1 and corresponds to a soft-in-plane fully flexible blade with uniform mass and stiffness. The data is intended to represent a helicopter configuration vaguely resembling an MBB-105 helicopter. The data in the table (except for C_w , γ and σ) have been nondimensionalized using M_b , L_b and $(1/\Omega)$ for mass, length, and time respectively. The control studies were obtained using a control flap centered about the 75% blade span position and extending over 12% of the blade span, with a chord equal to 25% of the blade chord. This configuration was found to provide levels of vibration reduction comparable to IBC (in which the entire blade undergoes cyclic pitch change) with control flap deflection angles less than 10° , which was considered a practical upper limit.

The minimum values of the quadratic cost functional obtained when implementing control through the ACF and IBC are presented in Fig. 2. The figure shows that very substantial vibration reduction was achieved by both control approaches over the entire range of torsional frequencies considered, and that the level of reduction produced by the actively controlled flap is comparable to IBC. In fact, for blades with a torsional frequency in range $3.1 \leq \omega_{T1} \leq 3.7$, which includes a considerable number of modern helicopter rotor blades, the level of vibration reduction produced by oscillating the relatively small trailing edge flap exceeds that achieved by oscillating the entire blade. This occurs when the torsional frequency of the blade ω_{T1} is close to the rotating frequency of the second flap bending mode, which is given by $\omega_{F2} = 3.7/\text{rev}$ when $x_c = 0.75R$.

A very important capability lacking in IBC, in which the entire blade undergoes a uniform pitch change about the blade root, is the ability to cyclically vary the twist

distribution of the blade. It was shown in Ref. 20 that cyclic variations in the blade twist could have a substantial impact on blade bending amplitudes. This may in part explain why oscillating a relatively small trailing edge flap can produce roughly the same degree of vibration reduction obtained by oscillating the entire blade. This implies that the control flap's ability to cyclically change the blade twist is responsible for its enhanced capability to influence, in a beneficial manner, the dynamic response of the blade.

Examination of Fig. 2 shows that the effectiveness of IBC is relatively insensitive to variations in the torsional stiffness of the blade, while the figure depicts a decrease in ACF effectiveness at the higher blade torsional frequencies. As the blade becomes stiffer in torsion, the ability of the control flap to affect the twist distribution of the blade is reduced, thus reducing its effectiveness in controlling vibrations. Practically, though, the value of the optimal cost functional at the higher torsional frequencies is still very small.

The degree of reduction obtained in the 4/rev hub loads by the ACF and IBC is compared in Figs. 3 and 4 for the torsional frequencies $\omega_{T1} = 3.5/\text{rev}$ and $\omega_{T1} = 5/\text{rev}$, respectively. For the torsional frequency $\omega_{T1} = 3.5/\text{rev}$, both control approaches successfully reduce the hub shears and moments by at least 95%. At the higher torsional frequency $\omega_{T1} = 5/\text{rev}$, the degree of reduction in the hub loads achieved by IBC is essentially unchanged; however, the ACF is slightly less effective, reducing the hub shears by only about 80%.

The maximum control angle amplitudes required for vibration reduction by the two control approaches are shown in Fig. 5. Of course larger control input angles are required by the ACF; however, these angles are quite reasonable. Over the entire range of blade torsional frequencies considered, the largest control flap deflection angle required was only 10° . Larger control input amplitudes are needed when the torsional stiffness increases, for both control approaches, as evident from Fig. 5; this behavior is also consistent with the observations made in Ref. 20.

A comparison of the power required to implement control through the ACF and IBC is presented in Fig. 6. The power required to drive the control surface actuators is defined by Eq. (19) and the power required to implement IBC is defined by Eq. (20). Figure 6 reveals that oscillating the entire blade requires considerably more power than oscillating the relatively small trailing edge flap: IBC requires anywhere from 3 times (for a torsionally stiff blade) to 10 times (for a torsionally soft blade) more power than consumed by the ACF. An increase in power requirements for both control approaches with increasing torsional stiffness is evident from Fig. 6; clearly vibration reduction in torsionally stiff blades is a more costly proposition.

6.3. Influence of Control Flap Spanwise Location

In the results presented in the last section, the trailing edge flap was centered about the 75% span position (i.e., $x_c = 0.75R$). This is very close to the node position of the second flap and lead-lag bending modes of the flexible blade, and therefore one could assume that centering the trailing edge flap about this node point would minimize its potential for exciting these modes. The effect of changing the spanwise location of the ACF was examined by moving its centroid outboard to the 85% blade span position ($x_c = 0.85R$). Figure 7 presents a comparison of the vibration reduction effectiveness of the ACF for these two different spanwise locations. An increase in the minimized value of J by nearly 1%, which represents about a 5% increase in the minimized 4/rev hub loads, is evident when the flap is moved outboard, for blades with a torsional frequency in the vicinity of $\omega_{T1} = 4.4/\text{rev}$. This

torsional frequency is very close to the rotating frequency of the second lead-lag bending mode, which is $\omega_{L2} = 4.48/\text{rev}$ (for $x_c = 0.85R$). Figure 7 implies that moving the centroid of the trailing edge flap away from the node position of the second flap and lead-lag bending modes has a detrimental impact on the vibration reduction potential of the ACF when the second lag and first torsional frequencies are relatively close. The decrease observed in the minimized value of J at the higher torsional frequencies for $x_c = 0.85R$ implies that moving the ACF outboard of the node point improves its vibration reduction effectiveness on torsionally stiff blades.

The effect of the ACF spanwise location on the control flap angles required for vibration reduction is shown in Fig. 8. It appears that the decrease in control flap effectiveness in the vicinity of $\omega_{T1} = 4.4/\text{rev}$ is counterbalanced by a small decrease in the required control input amplitudes. This change is quite small and it is difficult to assess its significance. A small increase in the required control input amplitudes is evident in Fig. 8 in the vicinity of $\omega_{T1} = 4/\text{rev}$. This frequency is very close to the rotating frequency of the second flap bending mode, which is $\omega_{F2} = 3.97/\text{rev}$ (for $x_c = 0.85R$).

The effect of the ACF spanwise location on the power requirements is shown in Fig. 9. The increase in control angles in the vicinity of $\omega_{T1} = 4/\text{rev}$ is accompanied by about a 100% increase in power requirements. However, for blades relatively stiff in torsion ($\omega_{T1} > 4.5/\text{rev}$) power requirements decrease by up to 70%. Thus, for torsionally stiff blades, moving the control flap outboard toward the blade tip enhances the vibration reduction effectiveness of the ACF and reduces the power required for vibration suppression.

Figures 7-9 demonstrate that coupling of the fundamental torsional mode with the second flap and lag bending modes of the blade has a substantial influence on the vibration reduction effectiveness of the ACF, and this effect is quite sensitive to changes in spanwise location.

6.4. Influence of Mass Offset

For the results presented thus far, the offset X_{ic} between the control flap hinge axis and the center of gravity of the control flap has been assumed to be zero, i.e., the flap is mass balanced. However, this offset can have a substantial influence on the inertial hinge moment. Therefore, the effect on the vibration reduction potential of the control flap is studied by moving the c.g. of the control flap aft one-quarter chord. Moving the c.g. aft had almost no effect on the vibration levels. However, Fig. 10 shows that moving the c.g. toward the trailing edge of the control flap resulted in slightly lower control flap deflection input amplitudes for blades relatively soft in torsion. The most pronounced influence of the chordwise movement of the control flap c.g. is on the power requirements, as shown in Fig. 11. This figure shows that moving the control flap aft of the hinge point resulted in up to a 66% reduction in the power requirements in the case of blades relatively soft in torsion. However, almost no power reduction is obtained on torsionally stiff blades.

6.5. Effect of Hinge Moment and Compressibility Correction

The importance of the value of the hinge moment correction factor C_f used in the active control studies was studied by changing its value from $C_f = 0.6$, used for generating the majority of the results, to a more conservative value $C_f = 0.5$. The results, presented in Ref. 24, indicate that the 16.7% decrease in the value of C_f had almost no effect on the potential of the ACF to reduce vibrations; however, it resulted in a 15-20% increase in both the control input requirements and the power requirements.

A qualitative approximation of the effects of compressibility on the performance of the ACF can be obtained using the Prandtl-Glauert correction factor. These results, presented in Ref. 24, indicate that for $\mu = 0.3$ and a blade tip Mach number, in hover, $M_{tip} = 0.65$, compressibility has a minor effect on the vibration reduction and power requirements of the ACF. However, for higher values of μ or M_{tip} , the effects of compressibility increase significantly, as the tip region of the blade approaches transonic conditions.

6.6 Time Domain Simulation

The results obtained by solving the flexible blade equations of motion using the ODE solver DE/STEP are presented next. All time domain studies are performed using the data presented in Table 1, with the 12% span, 1/4 chord trailing edge flap centered about the 75% blade span position. Unless stated otherwise, the numerical integration is performed using an error tolerance of $ERR = 10^{-5}$. This error tolerance was found to yield sufficient accuracy without requiring excessive computer CPU time expenditures. All calculations were performed on an IBM ES9000 model 900 mainframe computer.

The optimal control strategy used in this study, and in the majority of helicopter vibration reduction studies[5-19], is based on a quasistatic frequency domain model of the helicopter response to control. This approach completely ignores the effects of transient blade dynamics. The validity of this model and its implications are studied by generating time histories of the helicopter response to control.

As a first step, the converged optimal control solution obtained using the HBT is applied in the open-loop mode starting from steady state conditions at time $t=0$. The time history of the quadratic cost functional J is compared in Fig. 12 with the minimum value obtained using the HBT. Figure 12 shows that the minimum vibration levels are not attained immediately after the control is applied, but only after 5-10 rotor revolutions; this delay is attributed to transient blade dynamics. This implies that when implementing control in the feedback mode, the update period of the discrete-time closed-loop controller must be sufficient to allow the transients dynamics to die out, so that the vibration levels can be accurately measured before feeding them back to the controller.

Next, closed-loop control is examined by applying feedback control starting from steady state conditions at $t=0$. The performance of the closed-loop controller, implemented in the time domain, is depicted in Fig. 13 for the controller update periods $t_s = 1T$ and $t_s = 2T$, where $T = 2\pi/\Omega$ is the rotor period. The figure shows that the selection of the update period of the discrete-time controller is very important. In the case where control is updated at the end of each revolution ($t_s = 1T$), Fig. 13 shows that the controller can become unstable, resulting in a dramatic increase in vibration levels. For the update period $t_s = 2T$, however, the feedback controller produces substantial vibration reduction.

The performance of the closed-loop controller is examined in greater detail in Fig. 14 for the controller update periods $t_s = 2T$, $3T$, and $4T$. The smoothest performance is obtained using the update periods $t_s = 3T$ and $4T$. For these two update periods, the closed-loop controller converges to the minimized vibration levels in about 20 revolutions, as shown in Fig. 14. This required roughly 40 seconds of CPU time. When performing control simulations using the HBT, however, the closed-loop controller required 3-4 iterations to converge to the minimized vibration levels, which represents roughly 90-120 seconds of CPU time. Comparing this to the 30 CPU seconds needed by the procedure DE/STEP shows that time domain simulation of the helicopter response to control is potentially more efficient, in terms of

CPU time, than using a frequency domain solution approach such as the HBT. This may lead one to conclude that time domain simulations of feedback control are superior to frequency domain simulations. Furthermore, in a more practical case one could have highly unsteady aerodynamics, such as dynamic stall, where time domain simulation may be the only feasible approach.

A time domain simulation of the closed-loop controller starting from zero initial conditions (at time $t=0$) is shown in Fig. 15. Though zero initial conditions are unrealistic in a practical situation, they are used here to represent an arbitrarily large initial disturbance to the system. The performance of the controller in the presence of such a large disturbance is studied for the update periods $t_s = 2T$, $3T$, and $4T$. The time history of the vibration levels with the controller turned off (i.e., no control) is also shown. Figure 15 shows that the performance of the controller with the update periods $t_s = 2T$ is very poor. However, the controllers with the update periods $t_s = 3T$ and $t_s = 4T$ attained steady state minimized vibration levels within 30 revolutions, requiring about 60 seconds of CPU time. This is still less than the 90-120 CPU seconds required by the HBT to converge to the minimized vibration levels. Thus time domain simulation appears to be more computationally efficient than the frequency domain approach.

Figures 12-15 indicate that an update period of at least three rotor periods is necessary to ensure controller stability. Sufficient time must be allowed for the low frequency transient dynamics to be adequately filtered from the measured 4/rev vibration levels before feeding them back to the controller. The lead-lag regressing mode, which is very lightly damped, is the lowest frequency dynamic mode present, having a fundamental period of roughly three rotor revolutions. Thus using an update period equal to at least one full period of the lead-lag regressing mode, i.e. three rotor revolutions, should increase the degree to which the transient dynamics are filtered out of the vibration measurement.

7. Magnetostrictive Actuation

A recent study[35] indicated that the practical implementation of an ACF may be feasible using magnetostrictive actuation based on Terfenol-D. Magnetostrictive materials such as Terfenol-D produce strain when subjected to a magnetic field. Motivated by Ref. 35, the feasibility of implementing this particular magnetostrictive approach to vibration reduction was studied. A schematic drawing of the magnetostrictive actuator, which is conceptually similar to that proposed in Ref. 35, is shown in Fig. 16. The feasibility study, presented in detail in Ref. 36, concluded that relatively light weight and low power magnetostrictive actuators can be developed which are capable of driving blade mounted control flaps for vibration reduction in helicopter rotors. The minimum mass actuator design summarized in Table 2 was determined in Ref. 36 to be capable of producing the control flap hinge moments and deflection angles necessary for vibration reduction. The total mass of Terfenol-D required for each actuator amounts to only about 1.2% of the blade mass. Accounting for the mass of the supporting structure, wire coil, and power transfer system, a conservative estimate of the total mass of the actuator would be five times this amount, or 6% of the blade mass.

Other approaches to the actuation of blade mounted control flaps are also being considered. Researchers at McDonnell Douglas Helicopters[37] are currently developing an experimental mechanical device to actuate a trailing edge flap located near the blade tip for the purpose of reducing vibrations or enhancing rotor performance.

8. Conclusions

The most important conclusions obtained in this study are presented below. These conclusions should be considered within the framework of the simplifying assumptions used.

(1) Comparing the vibration reduction effectiveness of the ACF with IBC revealed that both approaches are equally effective in producing substantial vibration reduction. Furthermore, comparing the power requirements of the two approaches showed that the ACF required substantially less power than IBC for its implementation. This validates the results of the first stage of the feasibility study which concluded that the ACF is a very attractive device for vibration reduction, both due to its power efficiency and because it has no effect on the airworthiness when compared to IBC.

(2) Comparisons of the vibration reduction effectiveness of the ACF with IBC, in which the entire blade undergoes a uniform pitch change, indicate that the control flap's ability to alter the twist distribution of the blade is a key factor in its success in producing substantial vibration reduction despite its relatively small size.

(3) A detailed examination of the influence of the blade torsional stiffness on the vibration reduction potential of the ACF shows that the best vibration reduction was obtained for blades with a torsional frequency in the range $3.0 \leq \omega_{T1} \leq 4.0$, when a high degree of coupling existed between the fundamental torsional mode and the second flap bending mode of the blade.

(4) It was found that the vibration reduction effectiveness and power requirements of the control flap are strongly influenced by its spanwise location, and also on the chordwise offset of the c.g. from the hinge axis.

(5) The importance of the aerodynamic hinge moment and compressibility correction on the vibration reduction potential of the ACF was also considered and it was found that these two parameters play a relatively minor role.

(6) Comparisons of the CPU time requirements of the frequency domain and time domain solution approaches indicate that time domain simulations may potentially be more efficient.

(7) It was found that the quasistatic assumption, frequently used in active control studies, is equivalent to the requirement that sufficient time be allowed for the transients to die out before measuring the vibration levels and feeding them back to the controller. Using an update period equal to one full period of the lowest frequency transient mode should effectively filter out the effects of the transient dynamics.

(8) Magnetostrictive actuation may be a viable approach for the practical implementation of the ACF using a Terfenol-D based actuator.

Aknowledgements

The first author wishes to aknowledge support from the NASA Graduate Student Researchers Program under NASA NGT-50444, and the second author is grateful for the support of NASA Ames Research Center under NAG2-477. Both authors express their gratitude to the grant monitor Dr. S. Jacklin for his support and encouragement during this research.

References

- 1) G. Reichert, Helicopter Vibration Control-A Survey, Vertica, Vol. 5, No 1, pp 1-20, 1981.
- 2) R.G. Loewy, Helicopter Vibrations: A Technological Perspective, AHS Journal, Vol. 29, October 1984, pp 4-30.
- 3) J. Shaw, Higher Harmonic Blade Pitch Control for Helicopter Vibration Reduction: A Feasibility Study, M.S. Thesis, Department of Aeronautics and Astronautics, MIT, 1967.
- 4) W. Johnson, Self-Tuning Regulators for Multicyclic Control of Helicopter Vibrations, NASA Technical Paper 1996, 1982.
- 5) R.B. Taylor, F.A. Farrar, and W. Miao, An Active Control System for Helicopter Vibration Reduction by Higher Harmonic Pitch, Proc. 36th AHS Annual Forum, Washington, D.C., May 1980.
- 6) J.A. Molusis, The Importance of Nonlinearity on the Higher Harmonic Control of Helicopter Vibration, Proc. 39th AHS Annual Forum, St. Louis, Missouri, May 1983, pp. 624-647.
- 7) M.W. Davis, Refinement and Evaluation of Helicopter Real-Time Self-Adaptive Active Vibration Control Algorithms, NASA CR 3821, August 1984.
- 8) L. Robinson, and P.P. Friedmann, Analytical Simulation of Higher Harmonic Control Using a New Aeroelastic Model, AIAA Paper No. 89-1321, Proc. 30th AIAA/ASME/ASCE/AHS Structures, Structural Dynamics and Materials Conference, Mobile, Alabama, April 1989.
- 9) L. Robinson, and P.P. Friedmann, A Study of Fundamental Issues in Higher Harmonic Control Using Aeroelastic Simulation, Journal of the American Helicopter Society, Vol. 36, No. 2, April 1991, pp 32-43.
- 10) K. Nguyen, and I. Chopra, Application of Higher Harmonic Control (HHC) to Rotors Operating at High Speed and Thrust, Journal of the American Helicopter Society, Vol. 35, No. 3, July 1990, pp 78-89.
- 11) J.A. Molusis, C.E. Hammond, and J.H. Cline, A Unified Approach to the Optimal Design of Adaptive and Gain Scheduled Controllers to Achieve Minimum Helicopter Vibration, Journal of the American Helicopter Society, Vol. 28, No. 2, April 1983, pp 9-18.
- 12) G. Lehmann, The Effect of Higher Harmonic Control (HHC) on a Four-Bladed Hingeless Model Rotor, Vertica, Vol. 9, No. 3, 1985, pp 273-284.
- 13) J. Shaw, A. Albion, E.J. Hanker, and R. Teal, Higher Harmonic Control: Wind Tunnel Demonstration of Fully Effective Vibratory Hub Force Suppression, Journal of the American Helicopter Society, Vol. 34, No. 1, January 1989, pp 14-25.
- 14) E.R. Wood, J.H. Powers, J.H. Cline, and C.E. Hammond, On Developing and Flight Testing a Higher Harmonic Control System, Journal of the American Helicopter Society, Vol. 30, No. 1, January 1985, pp 3-20.

- 15) W. Miao, S.B.R. Kottapalli, and H.M. Frye, Flight Demonstration of Higher Harmonic Control (HHC) on S-76, Proc. 42nd AHS Annual Forum, Washington, D.C., June 1986, pp. 777-791.
- 16) M. Polychroniadis, and M. Achache, Higher Harmonic Control: Flight Tests of an Experimental System on SA 349 Research Gazelle, Proc. 42nd AHS Annual Forum, Washington D.C., June 1986, pp. 811-820.
- 17) M. Kretz, Research in Multicyclic and Active Control of Rotary-Wings, Vertica, Vol. 1, No. 1/2, pp. 95-105, 1986.
- 18) N. Ham, Helicopter Individual-Blade Control and its Applications, Proc. 39th AHS Annual Forum, St. Louis, Missouri, May 1983, pp. 613-623. May 1983.
- 19) N.D. Ham, Helicopter Individual-Blade-Control Research at MIT 1977-1985, Vertica, Vol. 11, No. 1/2, pp. 109-122, 1987.
- 20) A.Z. Lemnios, and A.F. Smith, An Analytical Evaluation of the Controllable Twist Rotor Performance and Dynamic Behavior, Kaman Report R-794, 1972.
- 21) T. Millott, and P.P. Friedmann, Vibration Reduction in Helicopter Rotors Using an Active Control Surface Located on the Blade, AIAA paper No. 92-2451, Proc. 33rd AIAA/ASME/ASCE/AHS Structures, Structural Dynamics and Materials Conference Dallas, Texas, April 1992, pp 1975-1988.
- 22) T. Millott, T., and P. Friedmann, The Practical Implementation of an Actively Controlled Flap to Reduce Vibrations in Helicopter Rotors, Proc. 49th Annual AHS Forum, St. Louis, Missouri, May 1993, pp 1079-1092.
- 23) J. Shamie, and P. Friedmann, Effect of Moderate Deflections on the Aeroelastic Stability of a Rotor Blade in Forward Flight, Paper No. 24, Proc. 3rd European Rotorcraft and Powered Lift Aircraft Forum, Aix-en-Provence, France, September 1977.
- 24) T. Millott, Vibration Reduction in Helicopter Rotors Using an Actively Controlled Partial Span Trailing Edge Flap Located on the Blade, Ph.D. Dissertation, Mechanical, Aerospace and Nuclear Engineering Department, UCLA, December 1993.
- 25) J.M. Greenberg, Airfoil in Sinusoidal Motion in a Pulsating Stream, NACA-TN 1326, 1947.
- 26) _____, MACSYMA Reference Manual, Symbolics Inc., June 1986.
- 27) P. Friedmann, Rotary-Wing Aeroelasticity With Application to VTOL Vehicles, AIAA paper No. 90-1115, Proc. 31st AIAA/ASME/ASCE/AHS/ACS Structures, Structural Dynamics and Materials Conference, Long Beach, CA, April 2-4, 1990, pp 1624-1670.
- 28) R.B. White, and M. Landahl, Effect of Gaps on the Loading Distribution of Planar Lifting Surfaces, AIAA Journal, Vol. 6, No. 4, 1968, pp 626-631.
- 29) R. Gray, and D.E. Davies, Comparison of Experimentally and Theoretically Determined Values of Oscillatory Aerodynamic Control Surface Hinge Moment Coefficients, RAE Technical Report 72023, March 1972.

- 30) _____, IMSL Library Reference Manual, IMSL Inc., Houston, Texas, 1980.
- 31) L.F. Shampine, and M.K. Gordon, Computer Solution of Ordinary Differential Equations-The Initial Value Problem, W.H. Freeman and Co., San Francisco, CA, 1975.
- 32) D.A. Peters, M. Chouchane, and M. Fulton, Helicopter Trim with Flap-Lag-Torsion and Stall by an Optimized Controller, Journal of Guidance and Control, Vol. 13, No. 5, 1990, pp. 824-834.
- 33) W. Johnson, Helicopter Theory, Princeton University Press, 1980.
- 34) I. Papavassiliou, P.P. Friedmann, and C. Venkatesan, Coupled Rotor/Fuselage Vibration Reduction Using Multiple Frequency Blade Pitch Control, Paper No. 91-76, Proc. 17th European Rotorcraft Forum, September 24-26, 1991, Berlin, Germany, pp 91-76.1 to 91-76.44.
- 35) R. Fenn, J. Downer, D. Bushko, V. Gondhalekar, and N. Ham, Terfenol-D Driven Flaps for Helicopter Vibration Reduction, Proc. SPIC Smart Structures and Materials Conference, February 1993, New Mexico.
- 36) T. Millott, and P. Friedmann, Magnetostrictively Actuated Control Flaps for Vibration Reduction in Helicopter Rotors, Proc. 2nd International Conference on Intelligent Materials, June 5-8, 1994, Williamsburg, Virginia.
- 37) F. Straub, and B. Charles, A New Approach to Active Control, Proc. Aeromechanics Specialists Conference, San Francisco, California, January 19-21, 1994, pp 7.7-1 to 7.7-14.

TABLE 1

Nominal blade configuration

Dimensional Data

$R = 4.91\text{m}$
 $\Omega = 425\text{ RPM}$
 $M_b = 52\text{ kg}$

Flight Data

$\mu = 0.3$

Blade Data

$N_b = 4$	$e = 0.0$
$c_b = 0.05498$	$L_b = 1.0$
$I_{MB2} = 0.0000$	$I_{MB3} = 0.0004$
$\omega_{F1} = 1.123$	$a_o = 2\pi$
$\omega_{L1} = 0.732$	$C_{do} = 0.01$
$2.5 \leq \omega_{T1} \leq 5.0$	$C_{mo} = 0.0$
$\gamma = 5.5$	$\sigma = 0.07$

Helicopter Data

$C_w = 0.005$	$fC_{df} = 0.01\pi$
---------------	---------------------

TABLE 2

Minimum mass actuator design

Maximum stress:	σ_{\max}	= -5 MPa
Minimum stress:	σ_{\min}	= -10 MPa
Prestress:	σ_0	= -5.57 MPa
Minimum strut angle:	ϕ_{\min}	= 1°
Strut volume:	V	= 34 cm ³
Strut mass:	M	= 315 g
Strut diameter:	D	= 1.6 cm
Strut length:	L	= 16.9 cm
Lever arm length:	r	= 3.0 cm
Control stroke:	Δy	= 5 mm
Magnetostrictive strain:		= 1.167e-3
Maximum field strength:		= 500 Oe

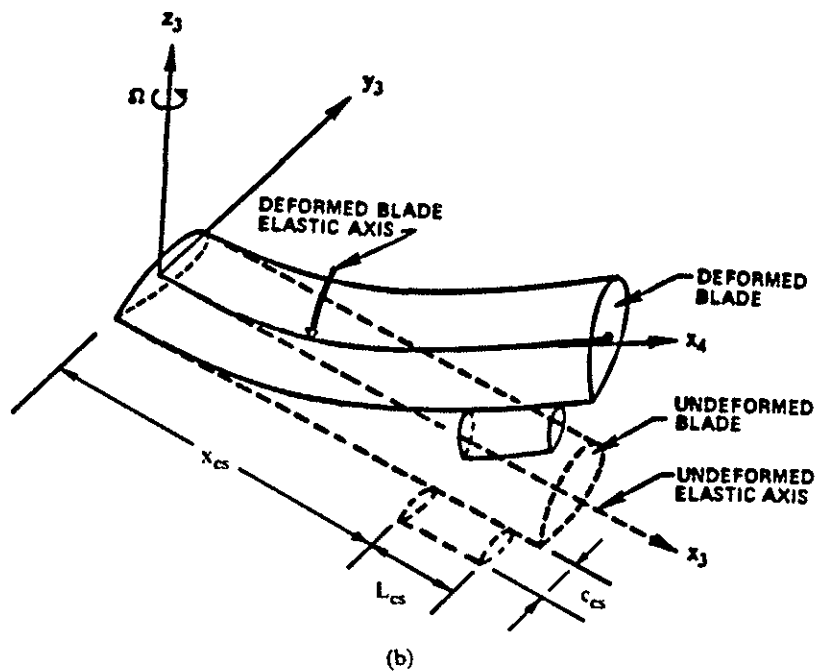
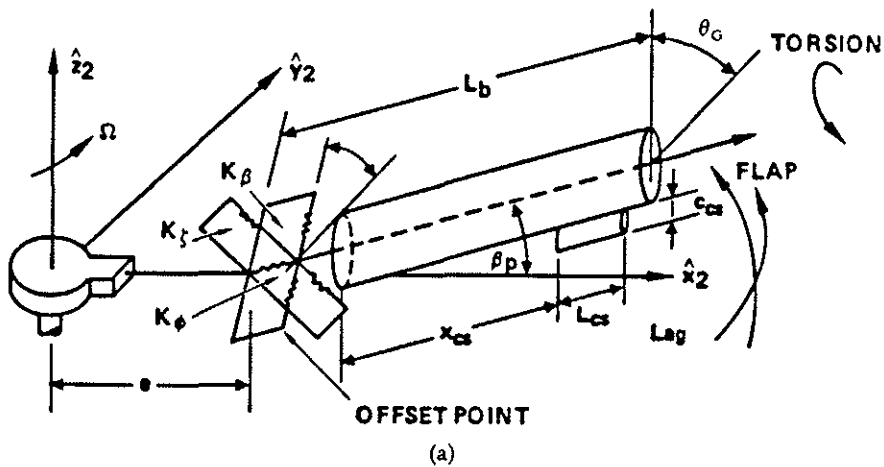


Figure 1: Rotor blade with trailing edge flap: (a) spring restrained blade (b) flexible blade

Controlled Cost Functional

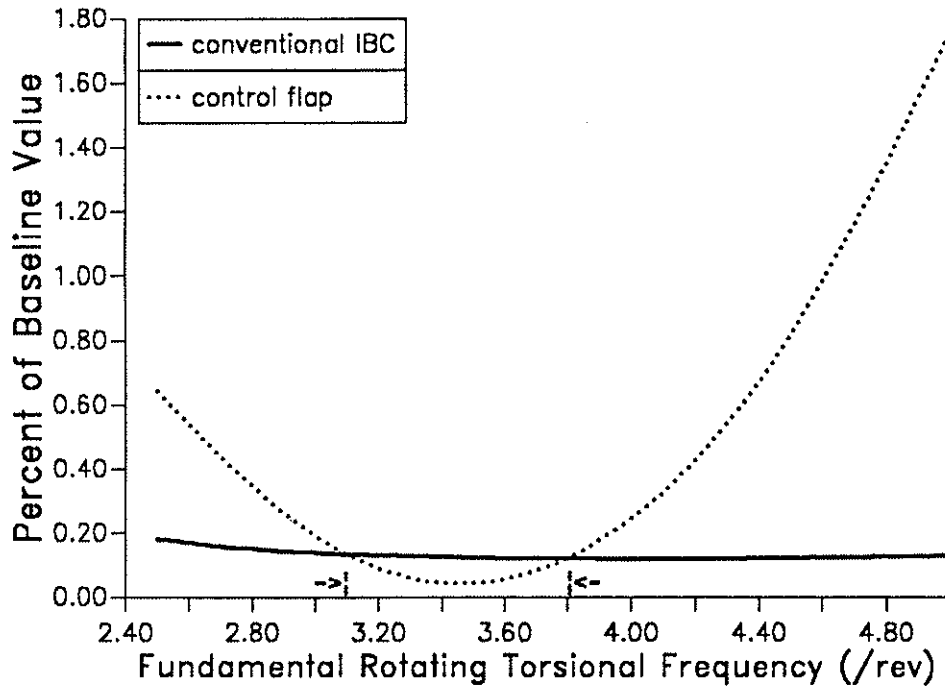


Figure 2: Minimized cost functional

Reduction of the 4/rev Hub Shears and Moments

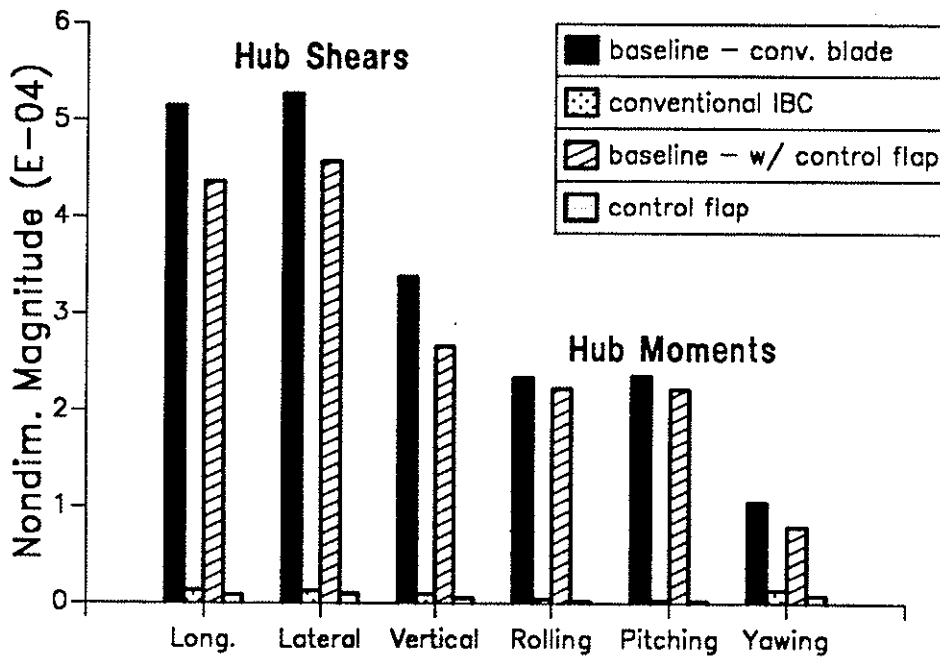


Figure 3: Minimized hub loads, torsional frequency = 3.5/rev

Reduction of the 4/rev Hub Shears and Moments

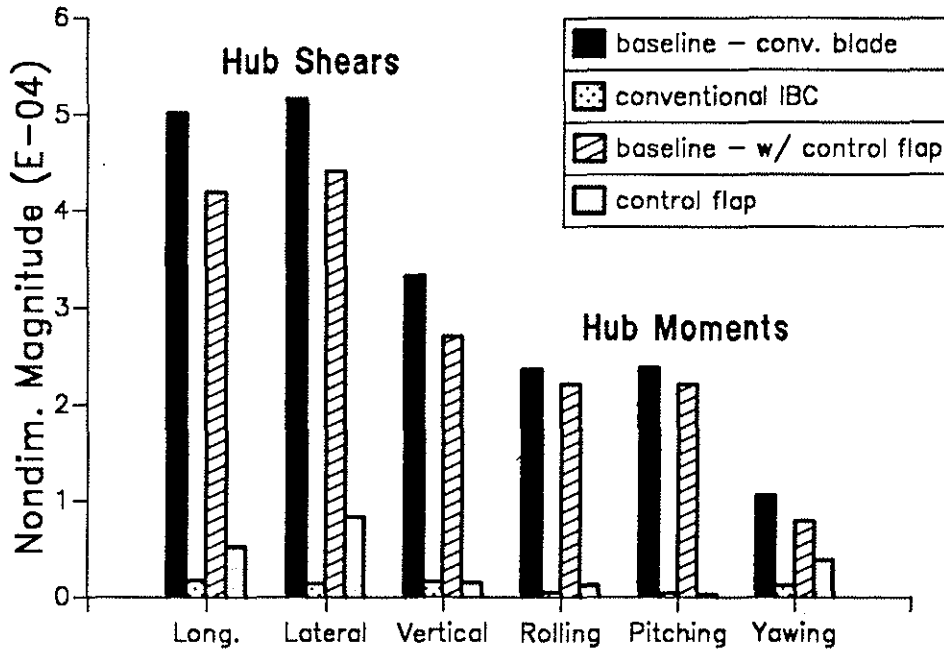


Figure 4: Minimized hub loads, torsional frequency = 5/rev

Control Input Requirements

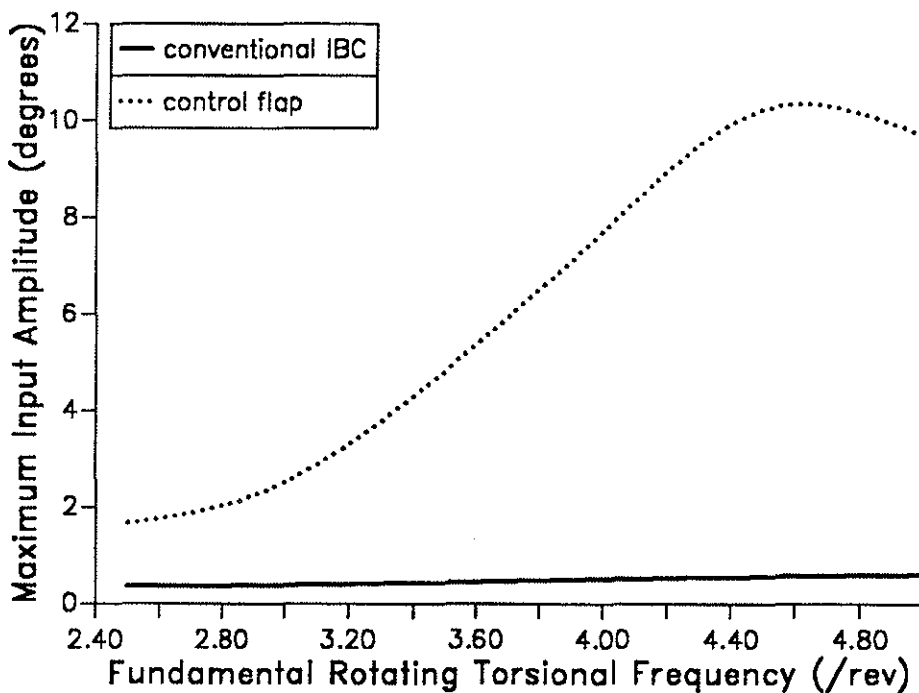


Figure 5: Control input requirements

Control Power Requirements

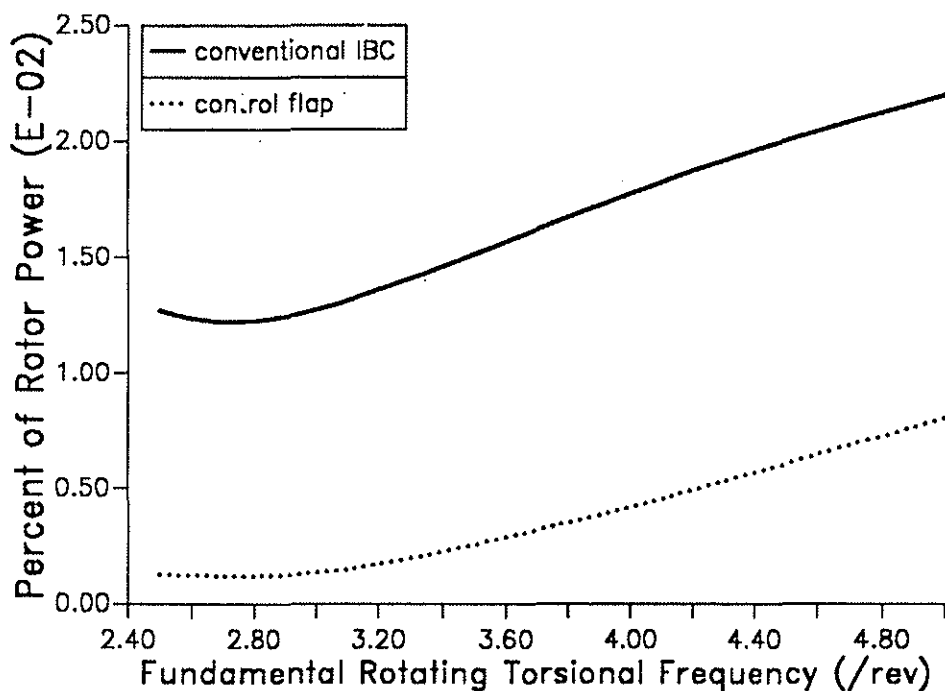


Figure 6: Control power requirements

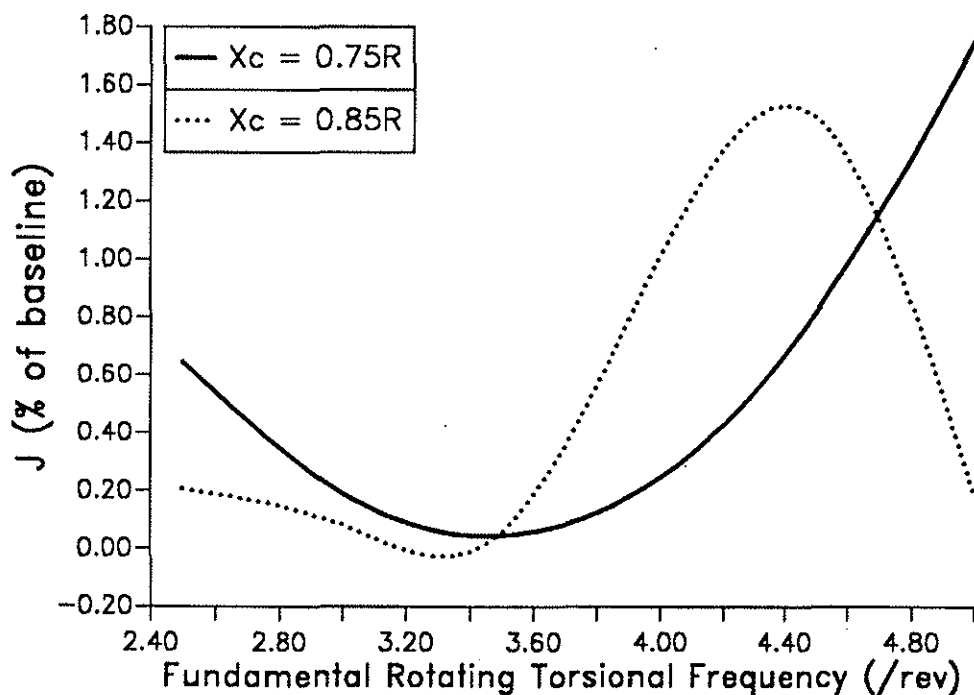


Figure 7: Effect of ACF spanwise location on minimized vibration levels

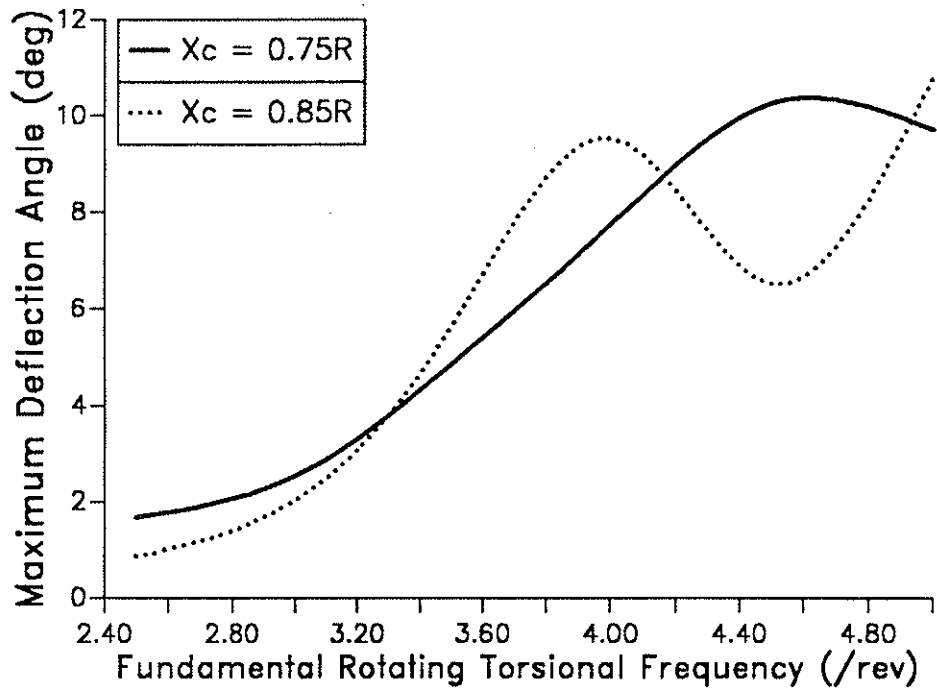


Figure 8: Effect of ACF spanwise location on control input requirements

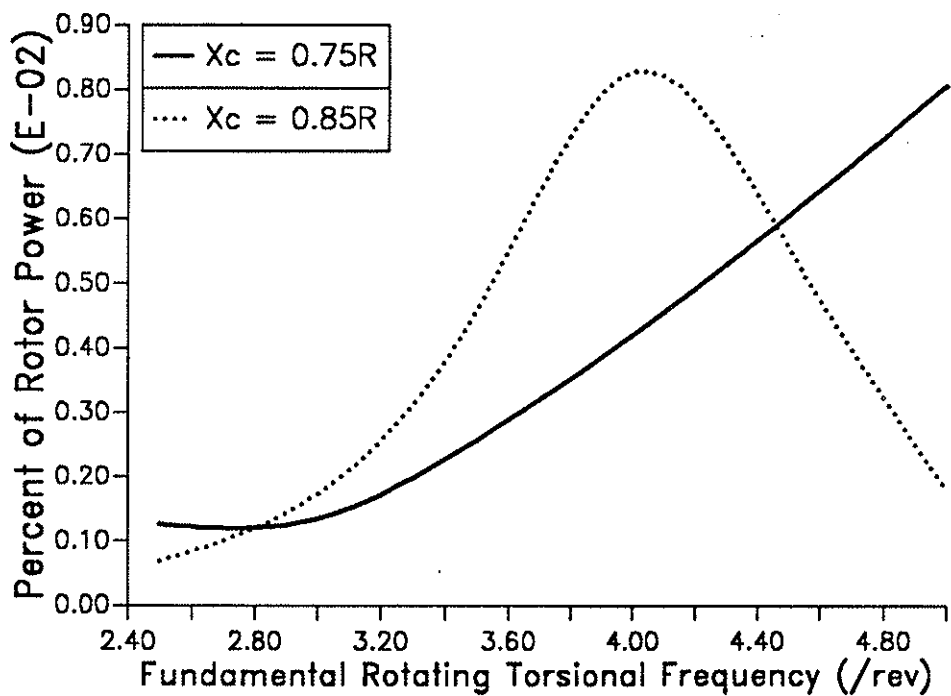


Figure 9: Effect of ACF spanwise location of control power requirements

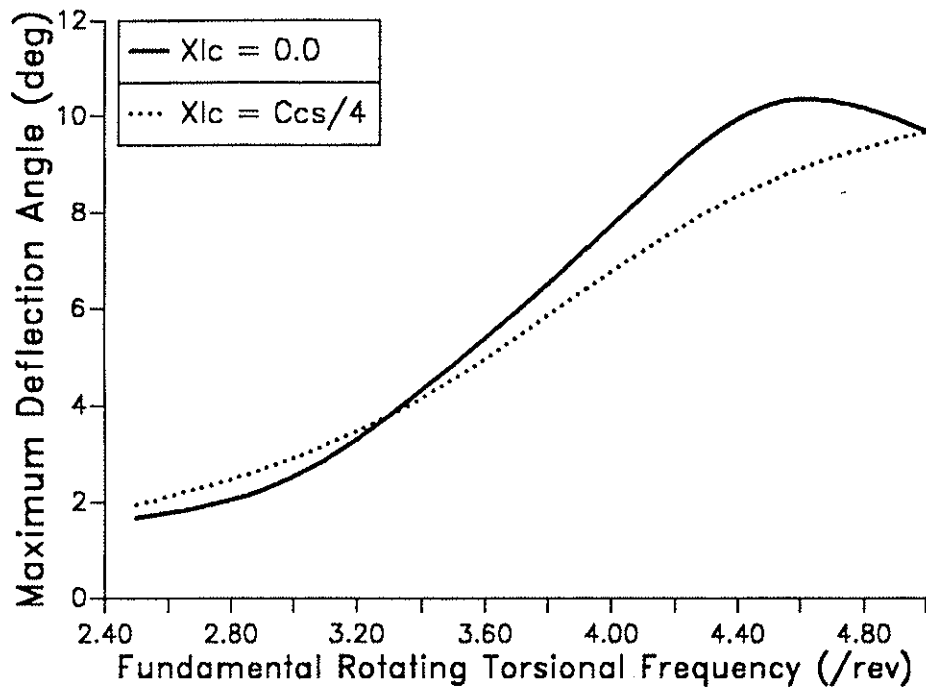


Figure 10: Effect of ACF mass offset on control input requirements

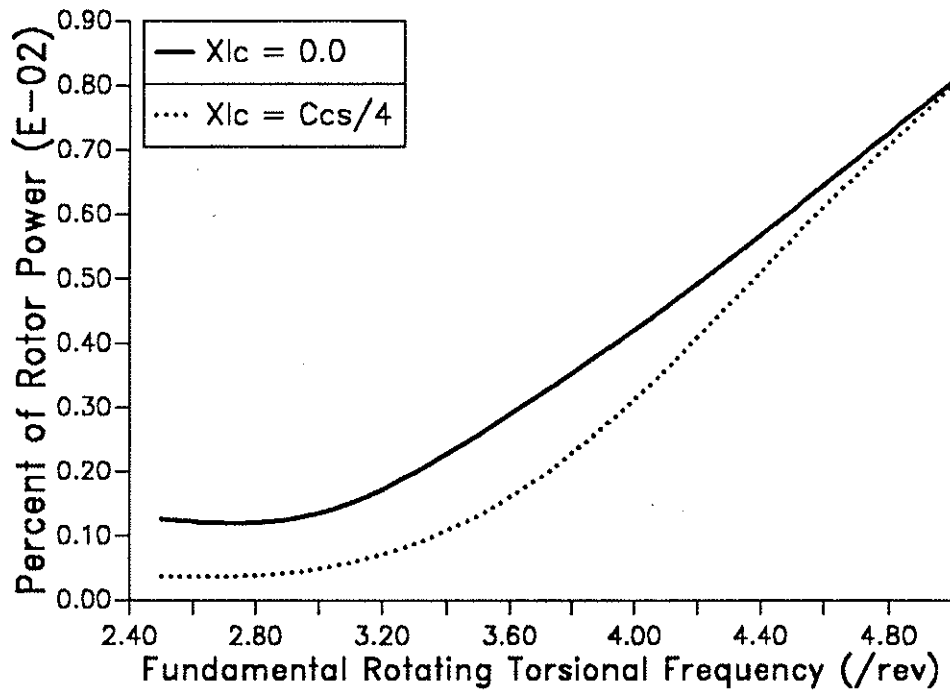


Figure 11: Effect of ACF mass offset on control power requirements

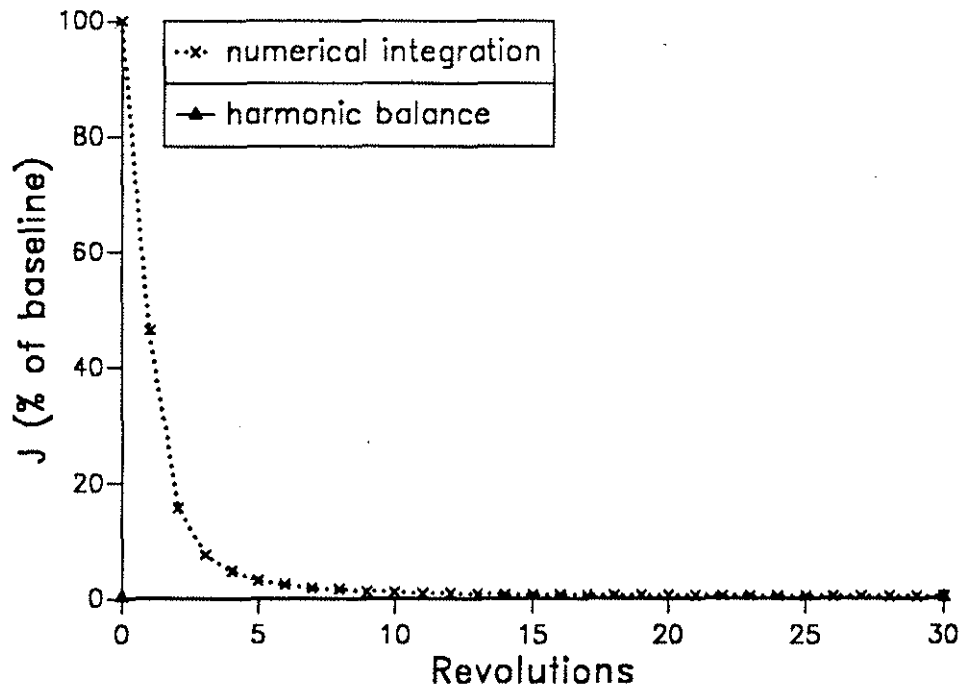


Figure 12: Time domain simulation of open-loop control

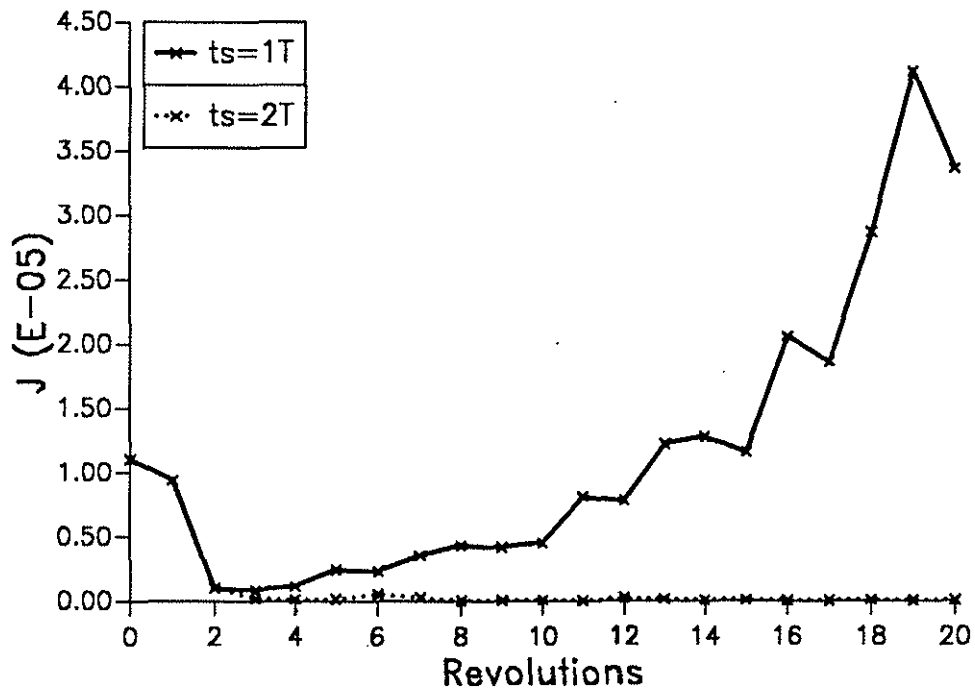


Figure 13: Closed-loop control from steady state conditions

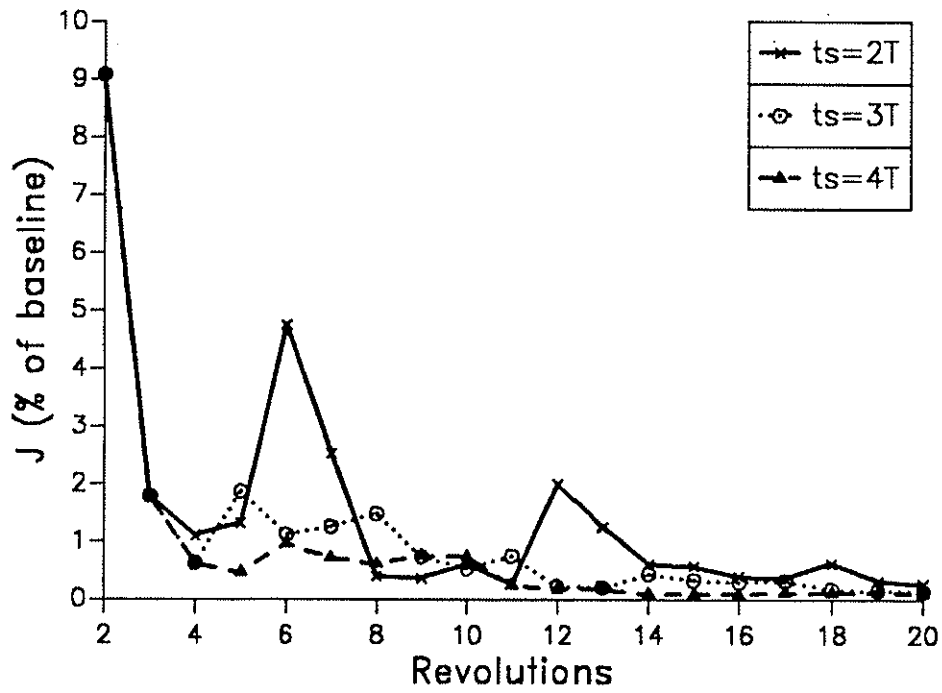


Figure 14: Closed-loop control from steady state conditions

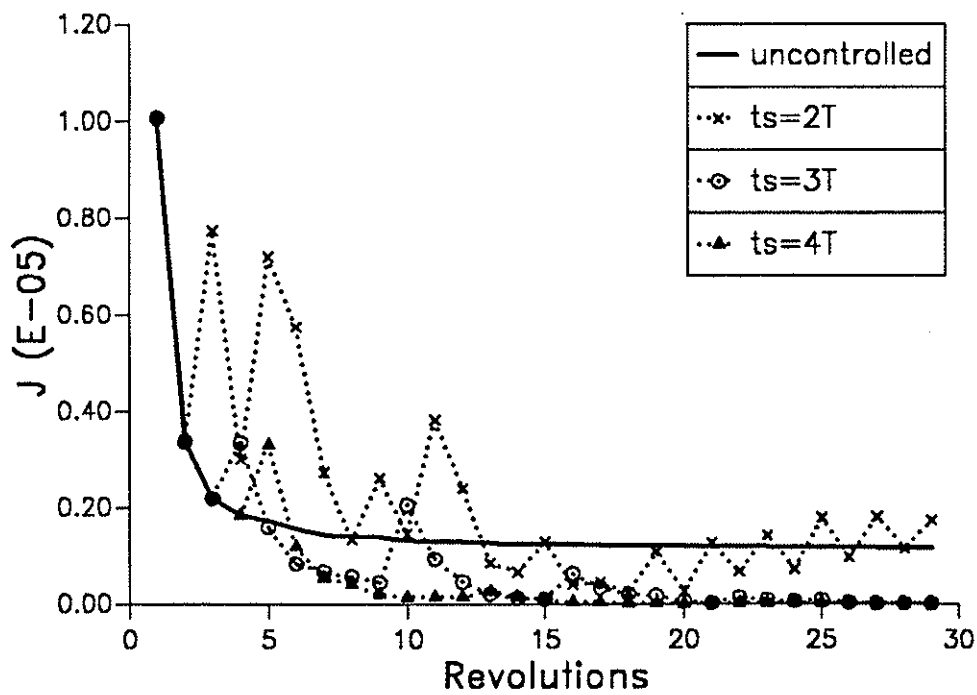


Figure 15: Closed-loop control from zero initial conditions

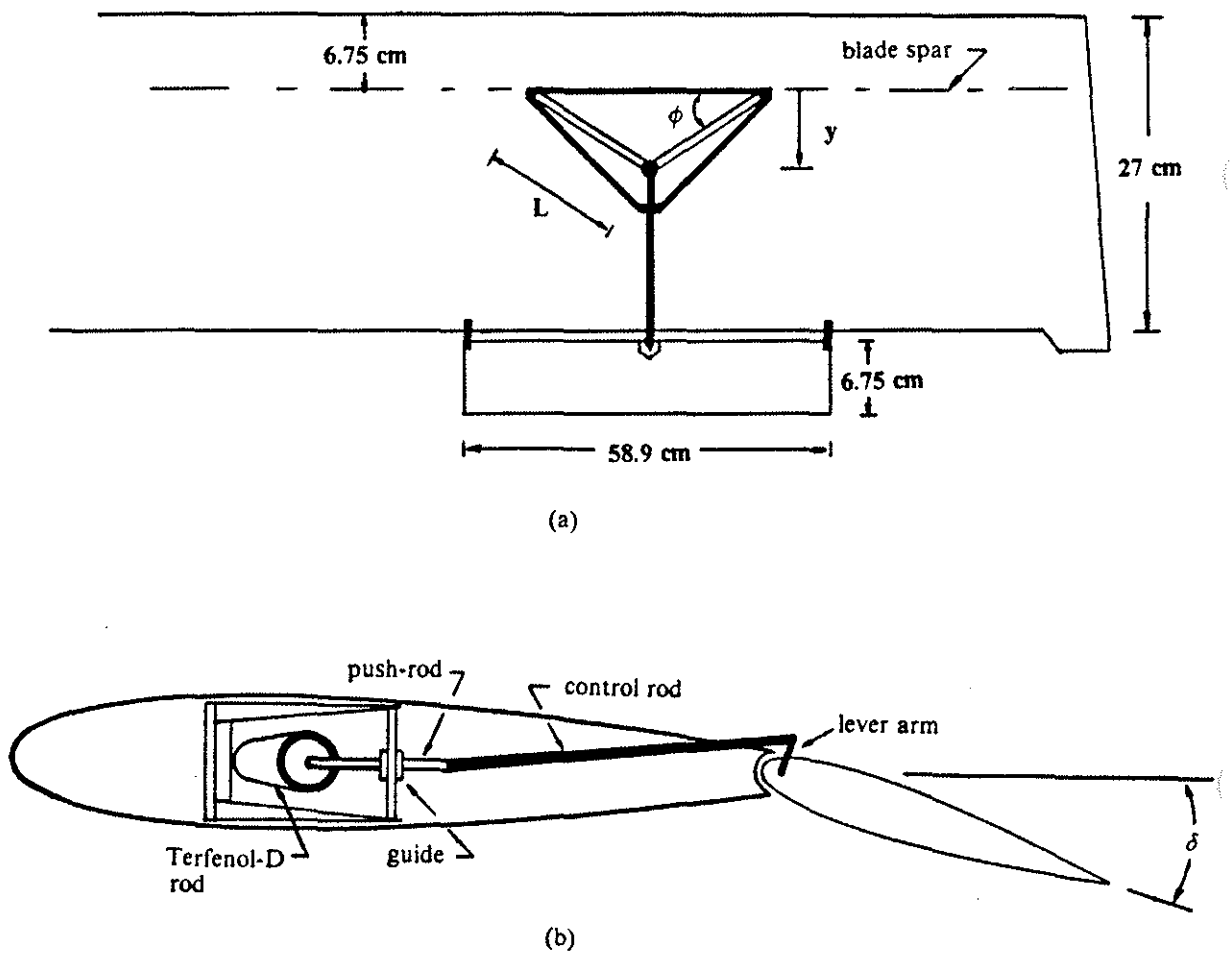


Figure 16: Schematic of magnetostrictive actuator: (a) top view (b) side view